

# Radial mixing of granular materials in a rotating cylinder: Experimental determination of particle self-diffusivity

Suman K. Hajra and D. V. Khakhar<sup>a)</sup>

Department of Chemical Engineering, Indian Institute of Technology—Bombay, Powai, Mumbai 400076, India

(Received 17 June 2004; accepted 8 October 2004; published online 1 December 2004)

Particle self-diffusion has a significant effect on mixing and thus on performance of rotating cylinder systems such as rotary kilns and drum mixers. We study experimentally the radial mixing of monodisperse beads of different colors in a quasi-two-dimensional cylinder rotated in the continuous flow regime. In this regime a shallow surface layer of particles flows steadily while the rest of the material rotates as a solid body. The initial distribution of tracer particles is taken to be radially symmetric and cylinder is taken to be half full. Both facilitate estimation of the particle self-diffusivity since the evolving concentration distribution during mixing in this case is radial for most part and the mixing in these conditions is shown to be dominated by diffusion of particles. A qualitative study of the mixing is carried out using digital photography. Radial number fraction profiles of the tracer particles are obtained by bulk sampling. Since mixing occurs only in the flowing layer, mixing is considered in terms of “passes” defined as the number of times the material in the bed entirely flows through the layer. Experimental results indicate that the mixing per pass decreases with increasing rotational speed, increases with increasing particle size, and is nearly independent of cylinder size. The mixed state captured by digital photography and the measured radial concentration profiles are well described by a convective diffusion model, using diffusivity as a fitting parameter. The diffusivity obtained from the model follows the scaling proposed by Savage [“Disorder, diffusion, and structure formation in granular flow,” *Disorder and Granular Media*, edited by A. Hansen and D. Bideau (Elsevier, Amsterdam, 1993), pp. 255–285] and a simple expression for the diffusivity is obtained in terms of the particle diameter and the static and dynamic angles of repose. © 2005 American Institute of Physics. [DOI: 10.1063/1.1825331]

## I. INTRODUCTION

Mixing of particles in rotating cylinders is important in a number of industrial systems such as rotary kilns and drum mixers.<sup>1,2</sup> The systems comprise a horizontal or slightly tilted cylinder partially filled with granular material. The cylinder rotates about its axis to generate granular flows in different regimes depending on the rotational speed. At low rotational speeds the material slips on the cylinder surface or flows as a series of discrete avalanches, while at higher rotational speeds the “rolling regime,” characterized by a steady, continuous flow is obtained.<sup>3</sup> Most practical systems operate in the rolling regime, in which the flow is confined to a shallow flowing layer of particles at the free surface while the remaining particles rotate as a fixed bed. Due to the simplicity of the flow, the rotating cylinder is also a useful prototype system to study the fundamental aspects of flow, mixing and segregation of granular materials.<sup>4</sup>

The large difference in relative mixing rates permits the consideration of the slow axial mixing and the relatively fast cross-sectional mixing, separately. Several previous studies have shown the axial mixing to be primarily due to particle diffusion.<sup>5,6</sup> Cross-sectional mixing, in contrast, is due to both convective mixing and diffusion. The relative contributions of the two depend on the fraction of the cylinder filled

with solids and the rate of convective mixing increases with decreasing fill fractions below 0.5.<sup>7</sup> The rate of mixing by convection is lowest when the cylinder is half full of particles (0.5 fill fraction). In many practical situations, for example, in rotary kilns, a very small axial mixing rate is required (to ensure equal residence times in the kiln) together with near complete cross-sectional mixing (to minimize temperature and composition inhomogeneities).<sup>8</sup> A quantitative estimate of particle self-diffusion in rotating cylinders is thus important from a practical viewpoint and is the focus of the present study. Since the flow is confined to a surface layer, convective and diffusive mixing occur only in the layer and there is no mixing in the rotating fixed bed. Furthermore, the diffusivity of particles is not an intrinsic property of the material but is determined by the flow, analogous to turbulent diffusivity. We thus determine the self-diffusivity under different conditions. The approach used here is based on tracer mixing experiments in the cross-section of the cylinder, using a quasi-two-dimensional batch system.

Estimates of the particle diffusivity in sheared granular flows were obtained by Savage<sup>9</sup> and Savage and Dai<sup>10</sup> from numerical simulations of shear flow of nearly elastic hard spheres. A scaling of the form

$$D = F(\nu)d^2\dot{\gamma} \quad (1)$$

was obtained, where  $d$  is the particle diameter,  $\dot{\gamma}$  is the shear rate, and  $F(\nu)$  is a function of the solid volume fraction ( $\nu$ ).

<sup>a)</sup>Electronic mail: khakhar@iitb.ac.in

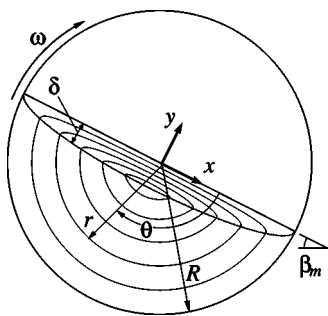


FIG. 1. Schematic view of the system showing the flowing surface layer and the rotating fixed bed. Streamlines of the flow are also shown.

Campbell<sup>11</sup> in more detailed simulations for a similar system showed that the diffusion is anisotropic and calculated the different components of the diffusivity tensor. All the components were found to be of similar magnitude. In this work we focus only on the component of the diffusivity normal to the streamlines (i.e., the  $D_{yy}$  component for the coordinate system defined in Fig. 1). This is the diffusivity reported in Ref. 9. Particle diffusivity in the rotating cylinder system has been directly estimated in only a few studies. Khakhar *et al.*<sup>7</sup> found order of magnitude agreement with the Savage<sup>9</sup> scaling based on an analysis of tracer mixing experiments in a rotating cylinder by means of a continuum model. The model also made good predictions of the qualitative features of the mixed patterns observed. Recently Hill *et al.*<sup>12</sup> presented measurements of particle self-diffusivity in the surface flow in a rotating cylinder based on particle tracking measurements. The diffusivity was related to the mean velocity. Hsiao and Hunt,<sup>13,14</sup> Hsiao and Shieh,<sup>15,16</sup> and Hsiao and Yang<sup>17</sup> considered side-by-side flowing streams of particles of different colors in a vertical channel to obtain the diffusivity transverse to the flow. Choi *et al.*<sup>18</sup> have considered a similar system using particle tracking, and found the motion to be “superdiffusive” under some conditions. Other systems in which the diffusivity has been studied include chute flow,<sup>19</sup> vibrated layers,<sup>20,21</sup> and Couette flow.<sup>22,23</sup>

The rotating cylinder geometry is convenient for the experimental determination of diffusivity by means of tracer experiments. The flow in this case is well characterized: the velocity profile is nearly linear<sup>24–27</sup> and shear rate is constant along the layer, at least at low rotational speeds.<sup>28,29</sup> The volume fraction of particles is also constant.<sup>25</sup> Thus based on Savage’s<sup>9</sup> scaling the diffusivity should be constant in the flowing layer. Analysis of tracer mixing experiments using a convective diffusion model can then be used to estimate the diffusivity. Another advantage of the rotating cylinder system is that the tracer concentration profile in the rotating bed is a 10–20 fold magnification of the profile in the flowing layer as explained below. The layer thickness is typically  $0.05R$ – $0.15R$ , where  $R$  is the cylinder radius, and all the material flowing through the layer also flows through the fixed bed (see streamline pattern, Fig. 1). The layer profile is mapped after magnification into the bed, and thus tracer concentration measurements can be made in the bed with much greater accuracy than in the layer.

The objective of the present study is to obtain the self-

diffusivity of different size particles under varying operating conditions using tracer mixing experiments. The initial distribution of tracer used in the experiment is radially symmetric and the fractional filling is 0.5, so that the mixed patterns are radially symmetric in significant portions. The mixing is then for most part “radial” and results from diffusion normal to the streamlines of the flow. This simplifies analysis, as discussed in more detail in Sec. II. The paper is organized as follows. The continuum model for flow and mixing is discussed in Sec. II. Experimental details are given in Sec. III. Experimental results for varying system parameters are discussed in Sec. IV. Comparison of model predictions to experimental results are given in Sec. V and the conclusions are given in Sec. VI.

## II. THEORY

We consider a model for the description of mixing of tracer particles in a rotating cylinder taking a continuum approach. A schematic view of the system is shown in Fig. 1. The model is developed here for half full mixers since experiments focus on this case, however, it may be generalized to arbitrary filling. Mixing is assumed to be confined to the surface flowing layer and the rest of the particles rotate as a fixed bed. The diffusivity of particles is assumed to be constant in the layer, and diffusion in the direction of flow is neglected. The model is very similar to that of Khakhar *et al.*<sup>7</sup> and thus we present it in brief here.

The convective diffusion equation for mixing in the layer is

$$\frac{\partial f}{\partial t} + v_x \frac{\partial f}{\partial x} + v_y \frac{\partial f}{\partial y} = D \frac{\partial^2 f}{\partial y^2}, \quad (2)$$

whereas in the bed, solid body rotation yields

$$\frac{\partial f}{\partial t} + \omega \frac{\partial f}{\partial \theta} = 0. \quad (3)$$

In the above equations  $f$  is the number fraction of the tracer particles,  $(v_x, v_y)$  is the velocity field in the layer,  $D$  is diffusivity, and  $\omega$  is the angular velocity of the cylinder. The coordinate system used is shown in Fig. 1. In Eq. (2), it is assumed that diffusion in the flow direction ( $x$  direction) is negligible relative to convection in that direction. Although the magnitude of the self-diffusivity in the flow direction ( $D_{xx}$ ) is larger than that perpendicular to the flow direction ( $D_{yy}$ ),<sup>11</sup> diffusion in the flow direction has little effect on mixing since transport in this direction is dominated by convection. In Eq. (3) the velocity field in the rotating fixed bed is taken to be  $(v_r, v_\theta) = (0, \omega r)$ .

We use the flow model of Khakhar *et al.*<sup>28</sup> in which the velocity field in the layer is

$$v_x = \dot{\gamma}(\delta + y), \quad (4)$$

$$v_y = \omega x(y/\delta), \quad (5)$$

where  $\delta$  is the layer thickness, given by

$$\delta = \delta_0 \left[ 1 - \left( \frac{x}{R} \right)^2 \right]^{1/2}, \quad (6)$$

and the midlayer thickness ( $\delta_0$ ) is related to the shear rate by

$$\delta_0 = \left( \frac{\omega}{\dot{\gamma}} \right)^{1/2} R. \quad (7)$$

The model is valid for low rotational speeds when the layer profile is symmetric and the shear rate is nearly constant and given by

$$\dot{\gamma} = \left[ \frac{g \sin(\beta_m - \beta_s)}{cd \cos \beta_s} \right]^{1/2}, \quad (8)$$

where  $g$  is acceleration due to gravity,  $c \approx 1.5$  is an empirical constant,  $\beta_m$  is the dynamic angle of repose, and  $\beta_s$  is the static angle of repose. Substituting for the shear rate expression in Eq. (7) we get

$$\delta_0 = (csFr/A)^{1/4} R, \quad (9)$$

where  $s = d/R$  is the size ratio,  $Fr = \omega^2 R/g$  is the Froude number, and  $A = \sin(\beta_m - \beta_s)/\cos \beta_s$ . The shear rate and the layer thickness can thus be estimated if measurements of  $\beta_m$  and  $\beta_s$  are available. We note that the flow model presented is an approximation of the actual physical system in which the boundary between the bed and the layer is diffuse. Although the velocity profile is linear for most part, it decays exponentially with depth in the bed near the boundary.<sup>25,26,30</sup> The region of exponential decay is relatively small and is neglected in the model.

The streamlines obtained by integrating the velocity field are shown in Fig. 1. The streamlines in the fixed bed region are arcs of circles as might be expected from the flow field. In the case of half full mixers, the streamlines are nearly semicircles and the residence time of all particles in the bed is nearly the same and approximately equal to the time for half a revolution. The residence time in the layer is small compared to that in the bed. Thus, in half a revolution, all particles pass through the layer just once and experience roughly the same extent of mixing. Consequently, we analyze mixing in terms of the number of “passes” rather than time of mixing. For arbitrary times of mixing and 50% filling, the bed would contain some particles that have passed through the layer  $n$  times and others which have passed through  $(n+1)$  times resulting in a concentration profile in the bed that is dependent on the azimuthal angle ( $\theta$ , Fig. 1).

Since the focus of the present work is on determining the diffusivity, the initial condition is chosen so that the effects of diffusivity on mixing are maximized and the contribution of convection is minimized. Thus the initial distribution of the tracer particles is taken with the boundary of the tracer volume tangent to the streamlines nearly everywhere, so that the gradient of the tracer concentration is normal to the streamlines ( $\mathbf{v} \cdot \nabla f = 0$ ). For the present case this corresponds to a semicircular shape with the center of the semicircle at the axis of the cylinder (Fig. 2). The tracer boundary is then tangent everywhere to the streamlines except in the layer. Since the streamlines are independent of  $\theta$ , the mixed state after a given number of passes is also independent of  $\theta$ ,

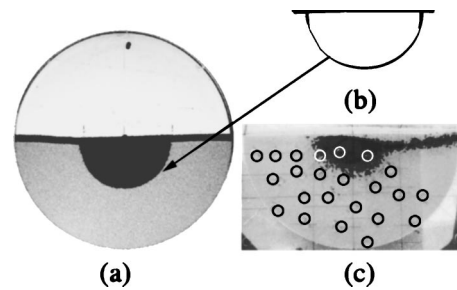


FIG. 2. (a) Initial distribution of tracer particles, (b) steel template used for generating the initial distribution of tracer particles, and (c) mixed state prior to sampling with the face plate replaced by the sampling plate with 23 holes at different locations.

omitting the discrepancy caused by the particles in the layer. For particles initially in the bed, mixing is purely radial and it is possible to characterize the mixing by the radial concentration profile  $f(r)$ .

We consider a simple model for the diffusivity based on the scaling proposed by Savage,<sup>9</sup> [Eq. (1)]. Since  $\dot{\gamma}$  and  $\nu$  are constant in the flowing layer,  $D$  is also a constant. Substituting for the expression for the shear rate using Eq. (7) we obtain

$$D = C_1 \omega R^2 d^2 / \delta_0^2. \quad (10)$$

The validity of the model presented above is considered by comparison to experiments.

We simulate mixing in the cylinder using Lagrangian simulations. This involves tracking the motion of a large number of tracer particles, of two different colors, starting with the particles arrayed in the specified initial state. Each particle trajectory is calculated independent of the others, by integrating the velocity field. Diffusion in the layer is simulated by giving the particles Gaussian random steps in the  $y$  direction with a mean square displacement of  $2D\Delta t$ , where  $\Delta t$  is the time step. Each trajectory for a given mixing time comprises a sequence of flow steps in the bed and the layer. When the particle is in the layer  $\{y \in [0, -\delta(x)]\}$ , the trajectory is calculated by integrating the following equations using the Euler method:

$$\frac{dx}{dt} = \dot{\gamma}(\delta + y), \quad (11)$$

$$\frac{dy}{dt} = \omega x \left( \frac{y}{\delta} \right) + G(D\Delta t), \quad (12)$$

where  $G(D\Delta t)$  is the Gaussian random step. If in a particular time step the particle moves from the layer into the bed, the time and the position at which the particle is at the bed-layer interface  $[y = -\delta(x)]$  is determined using the Newton–Raphson method. The particle is then assumed to be in the bed and is mapped to its new position by a solid body rotation. If sufficient mixing time remains, the particle is mapped to the symmetric position on the bed-layer interface where it reenters the layer. Otherwise, it is mapped within the bed, rotated by an angle determined by the time remaining, and the trajectory ends. The typical time step used in numerical integration is  $\Delta t = (2\pi/\omega) \times 10^{-4} \text{ s}^{-1}$  and the relative error in

the Newton–Raphson minimization is set to  $10^{-6}$ . A sufficiently large number of particles (about 16 000) are taken to calculate reasonable average number fraction profiles. The mixed state and the radial number fraction profiles are computed for one, two, and three passes. More details of the computational procedure are given in Khakhar *et al.*<sup>7</sup>

### III. EXPERIMENTS

Mixing experiments were performed in a quasi-two-dimensional cylinder of diameter 32 cm and length 1 cm. The cylinder end plates were made of transparent acrylic and the cylinder was made from an acrylic spacer sheet with a circular disk cut out. The plates and spacer were clamped together by bolts. The assembly could be easily removed from the rotary drive and the face plate could also be removed for arranging the tracer particles initially as well as for sampling. A computer controlled stepper motor with a sufficiently small step was used to rotate the cylinder. Spherical glass beads of mean sizes 1, 2, and 3 mm were used.

The glass beads were dyed with different colors (red and green) as described below. Drops of permanent ink (Camlin) were added into a desired volume of acetone and then the beads were poured into the solution and stirred. The solution was then kept undisturbed for about 4 h so that beads were uniformly coated with ink and then beads were spread on a tray and rubbed mildly with soft cloth to remove the excess quantity of the colored solution. The process resulted in a thin uniform coating of the dye on the bead surface which yielded beads of a uniform color intensity and free of stickiness.

The initial arrangement of the red and green particles was done using thin, stainless steel templates (Fig. 2) of height equal to the length of the cylinder (1 cm). The cylinder with its face plate removed was placed on an inclined surface. The template was placed at the center of the cylinder and filled with red glass beads. The rest of the half cylinder was filled with green glass beads of same size. The components were preweighed to ensure that the cylinder was 50% filled and the red particles completely filled the template. The face plate of cylinder was fitted and the assembly was made vertical to settle the particles. The assembly was again placed on the inclined surface and the face plate removed. The template was carefully removed and the face plate fitted back to obtain the initial condition as shown in Fig. 2. As discussed in the preceding section, with such an initial condition, the concentration profile of tracer after mixing is expected to be radial for most part.

The dynamics of mixing at various speeds of rotation (2, 3, 6, and 12 rpm), and for different particle sizes were studied for different numbers of passes. The mixed state after each pass was characterized by the radial concentration profile measured in the region where the concentration was independent of the azimuthal angle ( $\theta$ , Fig. 1). To measure the concentration profile, the cylinder rotation was stopped after completing the desired number of passes. The cylinder was then removed from the drive, placed on the inclined surface and the face plate was replaced by a sampling plate with

twenty-three 11 mm holes at 13 different radial positions (Fig. 2). The holes were sufficiently far apart and the sequence of the sampling was such that sampling from one hole did not disturb the particles under neighboring sampling holes. To ensure that sampling was done only in the fixed bed region where the concentration profile was radial, no sampling points were included in a strip near the free surface and in the triangular wedge formed by the final avalanche when the cylinder rotation was stopped [Fig. 2(c)]. A closely fitting, knife-edged steel tube (ID 10 mm and thickness 0.25 mm) was inserted in turn in each sampling hole until it touched the bottom plate and only particles inside the tube were collected by means of a vacuum probe. This ensured that the volume of material sampled was precisely controlled and relatively small ( $\sim 0.8 \text{ cm}^3$ ).

The number of red and green beads in the sample were then counted to obtain the number fraction of the red glass beads ( $f$ ). The beads were placed on a white paper as background and were spatially separated for ease of automatic counting. A thin layer of sticky adhesive was applied on the paper before placing the beads to prevent the beads from rolling. The sample was photographed at different exposures (Nikon Coolpix 990) and the images were analyzed (Image Pro Plus). Normal exposure images were analyzed to obtain the total number of beads whereas overexposed photographs, which emphasized the red beads, were used to automatically count the number of red beads. Each experiment was repeated at least three times. As a result of multiple sampling at a given radius for each experiment and repetition of experiments, each data point reported is an average of at least six measurements and the standard deviation is shown in each case.

Photographs were taken at low shutter speeds when the cylinder was rotating at specified speeds to determine the layer thickness  $\delta_0$  and also to measure the dynamic angle of repose  $\beta_m$  (for details see Ref. 31). The dynamic angle of repose is the angle of the free surface near the cylinder axis when the cylinder is rotating. The static angle of repose  $\beta_s$ , the angle of the free surface of the static bed when rotating cylinder is suddenly stopped, was also measured from digital photography of the static system.

### IV. EXPERIMENTAL RESULTS AND DISCUSSION

The mixing of tracer particles for an increasing number of passes for a typical case is shown in Fig. 3. The corresponding simulated results are shown alongside and will be discussed in the following section. The experimental images shown were taken during cylinder rotation. The mixed state after one pass shows the red (dark) particles in a semicircular region along with a streak nearly parallel to the free surface. The streak is formed by the red (dark) particles initially in the flowing layer, but not within the streamline corresponding to the semicircular interface. The boundary between the red (dark) and the green (light) particles in the layer is sharp (Fig. 3) and corresponds to this streamline. With increasing numbers of passes the semicircular shape becomes more diffuse maintaining its radial symmetry. The streak also becomes more diffuse.

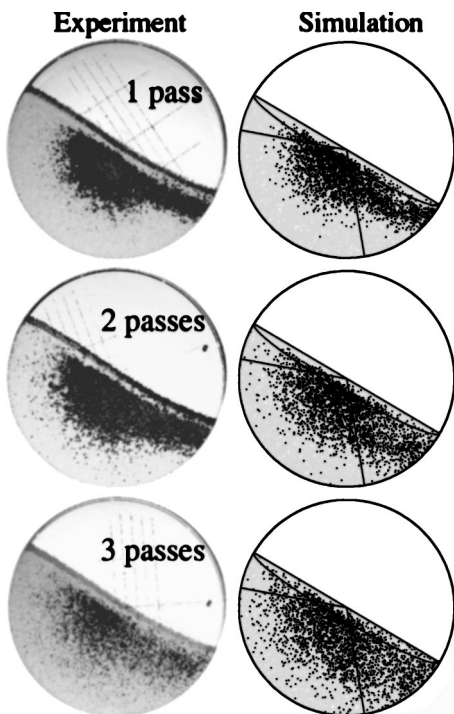


FIG. 3. Left column: Experimentally observed mixed states for 2 mm red (dark) and green (light) beads rotated at 2 rpm for different numbers of passes as indicated. Right column: Simulation results using the diffusivity and layer thickness given in Table I.

The number fraction variation with radial distance for the mixing experiments described above is shown in Fig. 4 for different numbers of passes. The concentration measurements are made in the region where the concentration distribution is radially symmetric. Each curve shown is an average of three experiments and the error bars show the standard deviation. Starting with a step concentration profile, the profile becomes flatter with each pass due to diffusive mixing. The profiles do not resemble those for classical Fickian diffusion in a slab, although the diffusion is Fickian in the layer, as shown below by means of comparison of model predictions to experimental profiles. This is because the bed profiles are a nonlinear mapping of the profiles in the flowing layer.

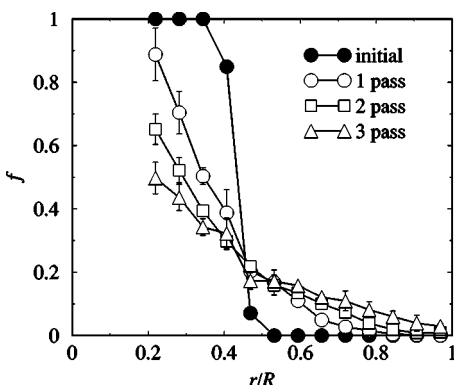


FIG. 4. Variation of the number fraction of red glass beads ( $f$ ) with scaled radial distance ( $r/R$ ) for 2 mm glass beads for different number of passes as indicated in the legend. The cylinder was rotated at 2 rpm.

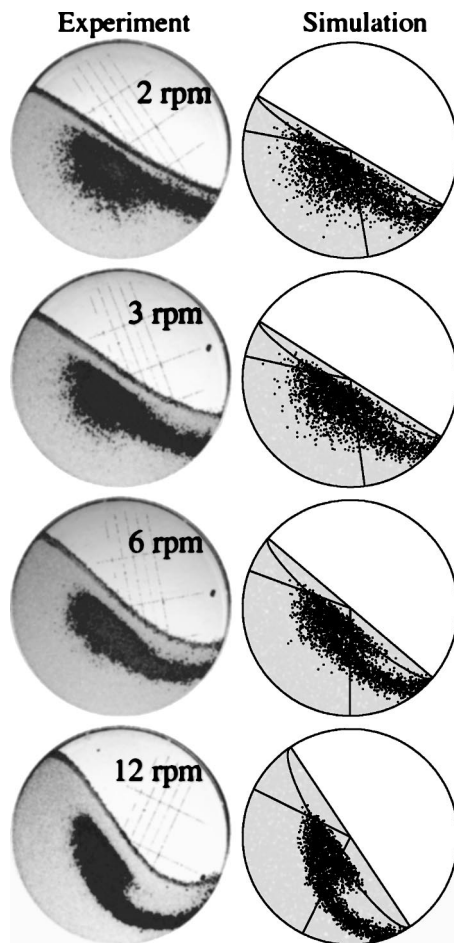


FIG. 5. Left column: Experimentally observed mixed states for 2 mm red (dark) and green (light) beads rotated at various speed of rotations as indicated. Right column: Simulation results using the diffusivity and layer thickness given in Table I.

The mixed states for one pass of 2 mm beads at different cylinder rotation speeds are shown in Fig. 5. The images show that the radial dispersion of particles decreases with increasing speed of rotation. The free surface is nearly flat at low rotational speeds and becomes increasingly curved with increase in rotational speed. This is reflected in the curvature of the radial streak which is nearly straight at low speeds but becomes increasingly curved at high rotational speeds. The measured number fraction profiles for one pass and at different rotational speeds are shown in Fig. 6. Although the profiles do not vary greatly with rotational speed, the profile for 12 rpm is significantly steeper than the profile for 2 rpm and the other profiles have intermediate slopes. Thus mixing per pass decreases with increasing rotational speed, which is in concurrence with the qualitative conclusion drawn from the images of the mixed state (Fig. 5).

The above results for varying rotational speed appear to be contrary to the expectation that the mixing rate, in general, should increase with rotational speed. However, the rate of mixing depends on both the mixing per pass and the number of passes per unit time. Hence the rate of mixing may increase with rotational speed even though the mixing per pass decreases.

We consider next, by means of simple arguments, why

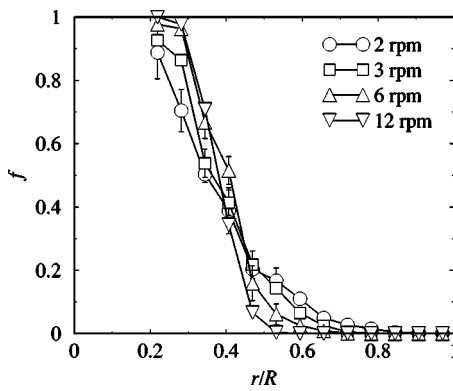


FIG. 6. Variation of number fraction of red glass beads ( $f$ ) with scaled radial distance ( $r/R$ ) after one pass for 2 mm glass beads for different speeds of rotation as indicated in the legend.

the mixing per pass reduces with rotational speed. As discussed earlier, the mixing in the system is dominated by diffusion since the boundary of the tracer volume coincides with a streamline. The typical length scale for diffusive mixing is

$$\eta \sim (D\tau)^{1/2}, \quad (13)$$

where  $\tau$  is the mean residence time of particles in the layer. Khakhar and Ottino<sup>8</sup> found  $\tau \sim 2\pi/\sqrt{\omega\dot{\gamma}}$  based on the velocity profile given in Eq. (4). Using the Eq. (10) for  $D$  and Eq. (7) for  $\dot{\gamma}$  we obtain

$$\eta \sim d \left( \frac{R}{\delta_0} \right)^{1/2}. \quad (14)$$

Calculations of  $\eta$  based on the above equation are given in Table I for the different cases studied using the measured values of the layer thickness  $\delta_0$ , also given in Table I. There is a decrease in  $\eta$ , indicating a reduction in mixing, with rotational speed (Experiments No. 3–6, Table I). Equation (13) indicates that  $\eta$  is proportional to the square root of both diffusivity  $D$  and the mean residence time  $\tau$ . The diffusivity increases with rotational speed (Table I); however, the mean residence time decreases faster (Table I), resulting in a de-

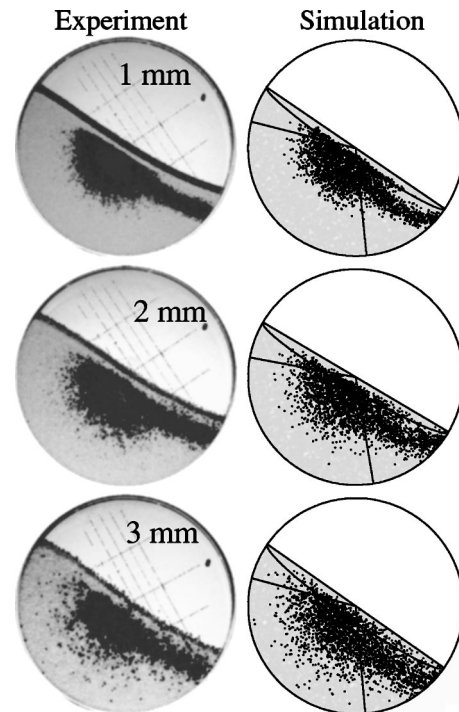


FIG. 7. Left column: Experimentally observed mixed states for red (dark) and green (light) beads rotated at 2 rpm for various sizes of glass beads as indicated. Right column: Simulation results using the diffusivity and layer thickness given in Table I.

crease in the mixing length. The physical model thus explains the somewhat unexpected experimental results for varying rotational speed given in Figs. 4 and 5. The number of passes per unit time is proportional to the rotational speed. Consequently, the overall rate of mixing is proportional to  $\eta\omega$ , which is found to increase with rotational speed (Table I), as expected.

Figure 7 shows the mixed state after one pass for three different particle sizes. The images show that the mixing per pass increases with particle size. The measured radial concentration profiles also show this trend (Fig. 8). Again the differences between the profiles are not large, and the data

TABLE I. Measured layer thickness  $\delta_0$ , static  $\beta_s$ , and dynamic  $\beta_m$  angles of repose and the fitted self-diffusivity  $D$  for different particle diameters  $d$  and cylinder rotational speeds  $\omega$ . The calculated layer residence time  $\tau$ , diffusional length  $\eta$ , and scaled diffusivity  $\bar{D}$  [Eq. (16)] are also given.

No.	$d$ (mm)	$\omega$ (rpm)	$\delta_0/R$	$\tau$ (s)	$\eta$ (mm)	$\eta\omega$ (mm/min)	$\beta_m$ (deg)	$\beta_s$ (deg)	$D$ (mm <sup>2</sup> /s)	$\bar{D}$
1	1	2	0.09	2.8	3.3	6.7	34.2±0.1	25.9±0.1	1.61	0.039
2	1	6	0.14	1.4	2.7	16.0	45±0.1		2.25	0.033
3	2	2	0.11	3.4	6	12.1	30.5±0.2	24.1±0.1	4.29	0.043
4	2	3	0.12	2.5	5.8	17.3	34.4±0.1		5.63	0.043
5	2	6	0.16	1.6	5	30.0	40.2±0.1		6.43	0.038
6	2	12	0.2	1.0	4.4	52.3	56.3±0.1		7.39	0.027
7	3	2	0.12	3.7	8.7	17.3	35.9±0.1	29.3±0.1	8.04	0.041
8	3	6	0.17	1.7	7.3	43.7	45±0.1		12.86	0.040

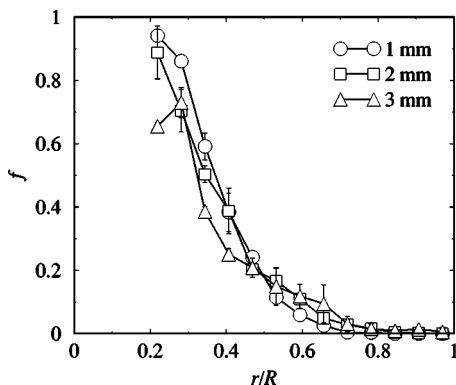


FIG. 8. Variation of number fraction of red glass beads ( $f$ ) with scaled radial distance ( $r/R$ ) after one pass for different sizes of beads as indicated in the legend. The cylinder is rotated at 2 rpm.

for the 3 mm particles have some scatter, however, there is a clear trend in terms of the steepness of the curves. Measurements show a slow increase of the layer thickness  $\delta_0$  with particle size (Table I, Experiment Nos. 1, 3, and 7). The diffusive length scale, however, is proportional to particle diameter [Eq. (14)] and increases with particle size (Table I, Experiment Nos. 1, 3, and 7) even though  $\delta_0$  increases. Thus mixing is faster for the large particles.

The diffusion of an annular strip after one pass is shown in Fig. 9. In this case there is simultaneous inward and outward radial diffusion of the tracer particles and a concentration peak is obtained in the profiles (Fig. 10). Experiments carried out for smaller diameter cylinders show that the mixing rate is nearly independent of cylinder diameter. The profiles for one pass are shown in Fig. 11. Only a subset of all the experimental results obtained are presented above so as to highlight the important physical phenomena and trends observed. However, all the results are used in the next section for determination of diffusivity.

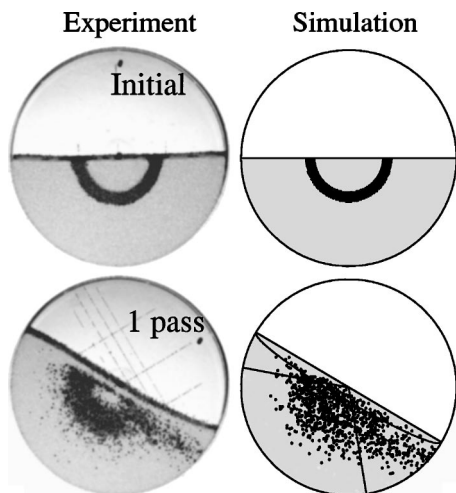


FIG. 9. Left column: Initial distribution of tracer particles and experimentally observed mixed states for 2 mm red (dark) and green (light) beads rotated at 2 rpm for one pass as indicated. Right column: Simulation results using the diffusivity and layer thickness given in Table I.

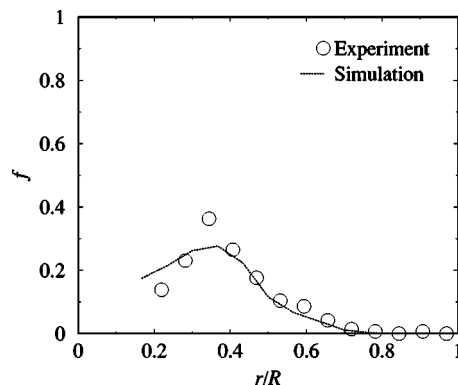


FIG. 10. Variation of the number fraction of red beads ( $f$ ) with scaled radial distance ( $r/R$ ) for 2 mm glass beads after one pass at 2 rpm for the annular strip initial condition. Symbols are experimental measurements and the line is the model prediction.

V. COMPARISON TO MODEL PREDICTIONS

The diffusivity is the only unknown parameter in the model described in Sec. II and is varied to obtain a fit of the model to experimental results. Starting with an initial condition identical to the experimental one, the time of rotation and diffusivity are varied to get a qualitative match with the experimental mixed state. The diffusivity value is then finely adjusted ( $\pm 10\%$ ) to obtain a match between the predicted and experimentally measured profiles. This procedure is carried out for each data set and each experiment yields a value of the diffusivity. For a particular set of system parameters profiles were obtained typically for three passes. The same fitted value of diffusivity gave good predictions of the concentration profiles for each pass.

Figure 3 shows the comparison between predictions and experiment of the mixed state for increasing numbers of passes. There is good qualitative agreement between the structures formed and the extent of dispersion. The differences between the two are primarily because a smaller number of particles are used in the simulation than the experiments. The comparison between theoretical and experimental radial concentration profiles given in Fig. 12 shows a good match between the two. The fluctuations in the predicted profiles are due to the relatively smaller number of particles

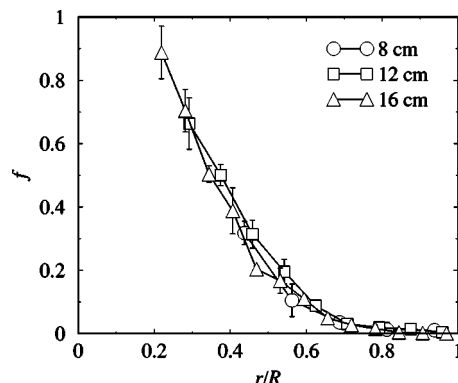


FIG. 11. Variation of the number fraction of red beads ( $f$ ) with scaled radial distance ( $r/R$ ) for 2 mm glass beads after one pass at 2 rpm for different cylinders radii as indicated in the legend.

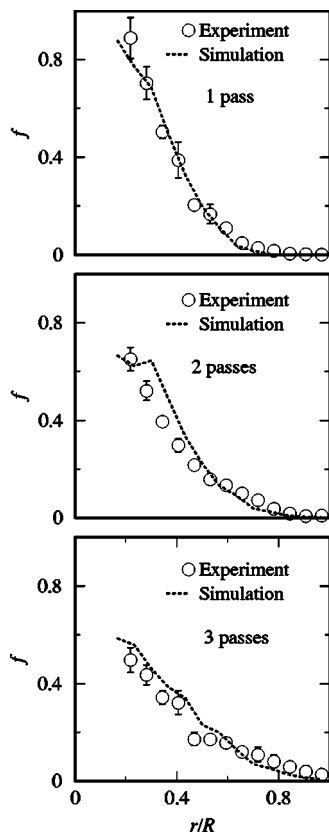


FIG. 12. Comparison of experimental and theoretical number fraction profiles for 2 mm glass beads rotated at 2 rpm for different number of passes as indicated in the legend. Parameters used in the simulation are given in Table I.

used in the simulation as compared to experiments as well as due to the reduction in number of particles used in calculating the concentration for the smaller radial distances.

Figure 5 shows similar qualitative agreement between theory and experiment. In this case the higher rotational speeds result in a significantly curved interface which is not taken into account in the theory but this does not appear to significantly affect the patterns. This conclusion is true even for the predicted radial concentration profiles (Fig. 13) which match the experimental profiles. The results indicate that curvature of the surface does not have a significant effect on mixing. This is analogous to boundary layer flows in which the curvature of the layer is unimportant because the layer is thin compared to its length. The effect of varying particle size is well described by the model both in qualitative (Fig. 7) and quantitative terms (Fig. 14).

The mixing in the case with an annular strip as the initial configuration is also described by the model reasonably well (Figs. 9 and 10). The predictions of the model deviate from the experimental results at smaller radii. The results indicate that the predicted inward diffusion flux (i.e., toward the inner streamlines) is higher than the experimental flux. This deviation between predictions and experimental measurements is a consequence of the gradual decrease of the velocity with depth in the bed rather than a sharp change at the boundary as assumed in the model. Thus the shear rate also decays slowly with depth resulting in lower values of the diffusivity

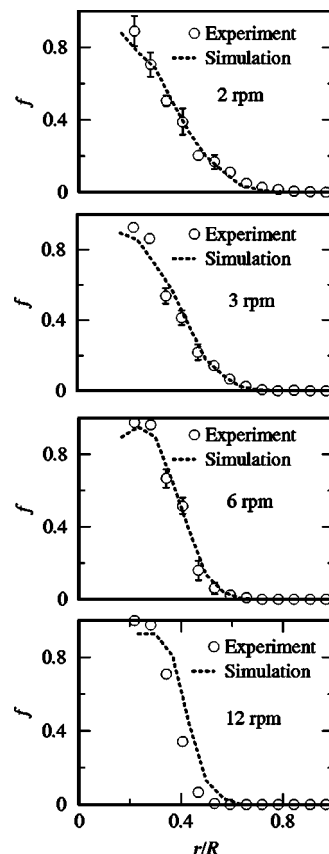


FIG. 13. Comparison of experimental and theoretical number fraction profile for 2 mm glass beads rotated at different rotational speeds for one pass as indicated in the legend. Parameters used in the simulation are given in Table I.

in regions of the layer corresponding to the inner streamlines. This results in the experimentally measured concentrations being lower than the predicted values at small radial distances (Fig. 10).

The fitted values of the self-diffusivity are given in Tables I and II for all the experimental cases considered. The magnitudes of the diffusivity values obtained are reasonable and compare well with those reported by Hill *et al.*<sup>12</sup> ( $\sim 10 \text{ mm}^2/\text{s}$ ). All the diffusivity data obtained are compared in Fig. 15 to the prediction of Eq. (10). The measured layer thicknesses used in the scaling are also given in Table I. The scaling works remarkably well for all the data generated with the constant in Eq. (10) given by  $C_1=0.065$ . The data span four particle sizes ( $d=1, 1.5, 2,$  and  $3 \text{ mm}$ ), four rotational speeds ( $\omega=2, 3, 6,$  and  $12 \text{ rpm}$ ), three cylinder radii ( $R=8, 12,$  and  $16 \text{ cm}$ ), and three passes in each case.

The scaling, as considered above, requires the measurement of the layer thickness, which is not straightforward. However, the model expression [Eq. (9)] can be used to estimate the layer thickness  $\delta_0$ . Figure 16 shows a comparison of the measured and experimental layer thicknesses. There is reasonable agreement between the two as shown previously.<sup>31</sup> The static and dynamic angles of repose used in the calculation of  $\delta_0$  are given in Tables I and II. The scaled diffusivity [Eq. (10)] using the model equation for the layer thickness [Eq. (9)] is

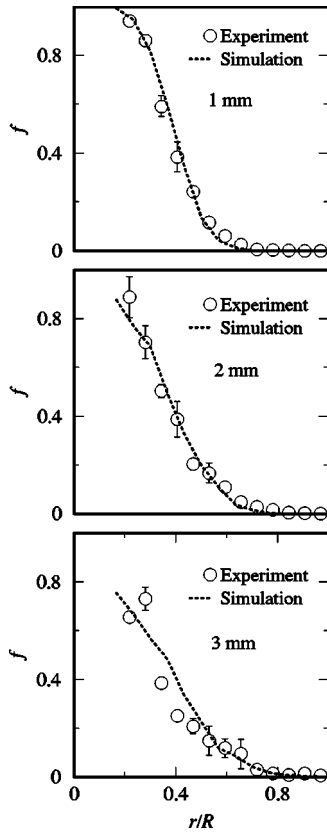


FIG. 14. Comparison of experimental and theoretical number fraction profiles after one pass and rotational speed 2 rpm for glass beads of different sizes as indicated in the legend. Parameters used in the simulation are given in Table I.

$$\frac{D}{\omega R^2} = C_2 \left( \frac{As^3}{Fr} \right)^{1/2}, \quad (15)$$

where the constant  $c$  is incorporated into the prefactor  $C_2$ . Figure 17 shows a comparison of the scaled measured diffusivity ( $D/\omega R^2$ ) with the predicted diffusivity using the calculated value of the layer thickness [Eq. (15)]. Again there is good agreement with  $C_2=0.041$ . The results indicate that the diffusivity may be calculated from Eq. (15), for a wide range of system parameters.

Expanding Eq. (15) into dimensional form we obtain

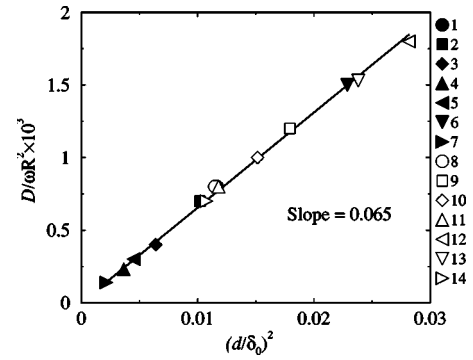


FIG. 15. Symbols show a comparison of the scaled diffusivity ( $D/\omega R^2$ ) obtained from experiments to the predictions of Eq. (10). The numbers in the legend indicate the data sets given in Tables I and II. The line is a least squares fit to the data.

$$D = C_2 d^{3/2} g^{1/2} \left( \frac{\sin(\beta_m - \beta_s)}{\cos \beta_s} \right)^{1/2} \quad (16)$$

$$\approx C_2 d^{3/2} g^{1/2} (\beta_m - \beta_s)^{1/2}. \quad (17)$$

We thus see that the diffusivity in a rotating cylinder system depends primarily on the particle diameter and the static and dynamic angles of repose. The diffusivity does not depend directly on rotational speed of the cylinder. However, increase in the rotational speed results in increase in  $\beta_m$  and thus the diffusivity increases with rotational speed. The diffusivity is independent of cylinder size. The above correlation for the diffusivity [Eq. (17)] is thus local and should be valid for surface flows, in general. The diffusivity scaled on the basis of Eq. (16) is

$$\bar{D} = D/[d(gdA)^{1/2}] = C_2, \quad (18)$$

and calculated values for each run are given in Tables I and II. The values are close to the fitted value (0.041).

## VI. CONCLUSIONS

We presented a detailed experimental study of mixing of tracers in the cross section of a quasi-two-dimensional rotating cylinder. A 50% cylinder filling and an initial distribution of tracer with the boundary of the tracer volume largely tan-

TABLE II. Fitted values of diffusivity  $D$  for different cylinder radii  $R$ , particle diameters  $d$ , and cylinder rotational speeds  $\omega$ . The calculated scaled diffusivity  $\bar{D}$  [Eq. (16)] is also given.

No.	$R$ (mm)	$d$ (mm)	$\omega$ (rpm)	$\delta_0/R$	$\beta_m$ (deg)	$\beta_s$ (deg)	$D$ (mm <sup>2</sup> /s)	$\bar{D}$
9	120	2	2	0.12	29.5±0.1	25.1±0.1	3.62	0.044
10	120	2	2.3	0.14	29.6±0.1		3.47	0.041
11	120	1.5	2.3	0.11	33.9±0.1		2.78	0.036
12	80	2	2	0.15	26.1±0.1	24.1±0.1	2.41	0.044
13	80	2	2.8	0.16	27.5±0.1		2.90	0.040
14	80	1	2.8	0.12	30.3±0.1		1.14	0.033

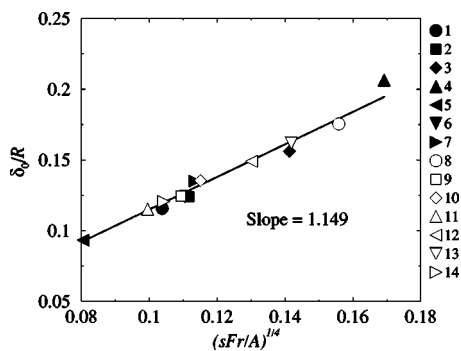


FIG. 16. Comparison of the measured layer thickness to the predictions of Eq. (9). The numbers in the legend indicate the data sets given in Tables I and II. The line is a least squares fit to the data.

gent to the streamlines are used so that mixing is dominated by diffusion rather than convection. The mixed state after different numbers of passes is analyzed by means of photographs and spatial sampling to obtain the radial concentration profiles. Experiments are carried out for different rotational speeds, particle sizes, and cylinder sizes. The mixing of an annular tracer strip is also presented.

The results indicate that the mixing per pass decreases with increasing rotational speed, increases with increasing particle size and is nearly independent of cylinder size. Some of these results are counter intuitive but are explained quite well in terms of a diffusional length scale obtained by means of physical arguments. The experimental results are analyzed using a continuum approach. The convective diffusion equation with the flow model of Khakhar *et al.*<sup>28</sup> is used. The particle diffusivity is the only unknown parameter of the model and is treated as a fitting parameter. The model gives good qualitative predictions of the mixed state and very good predictions of the radial concentration profiles. The fitted values of the diffusivity are well described by the Savage<sup>9</sup> scaling ( $D \sim d^2 \dot{\gamma}$ ) with the shear rate is obtained from the model of Khakhar *et al.*<sup>28</sup> The experiments indicate that the expression  $D = 0.041 d^{3/2} [g \sin(\beta_m - \beta_s) / \cos \beta_s]^{1/2}$  gives good predictions of the particle self-diffusivity over a wide range of system parameters.

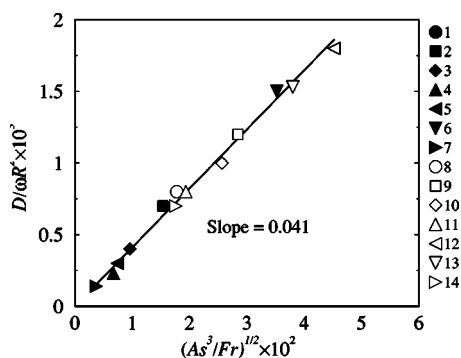


FIG. 17. Symbols show a comparison of the scaled diffusivity ( $D/\omega R^2$ ) obtained from experiments to the predictions of Eq. (15). The numbers in the legend indicate the data sets given in Tables I and II. The line is a least squares fit to the data.

The results presented show that a relatively simple continuum model gives a very good description of mixing in a rotating cylinder at least at a macroscopic scale. We note that the flow model becomes increasingly inaccurate with increase in rotational speed due to curvature of the surface and a nonsymmetric layer profile.<sup>28</sup> However, this does not appear to have a significant effect on mixing because the layer is thin relative to its length. The model should be useful for other surface flows, such as heap flows, given that the same flow model is valid for these systems.<sup>28,32</sup>

The behavior of the diffusivity is more complex at a particle scale compared to that at the macroscopic scale considered in this work. Measurements from individual particle trajectories indicate that the diffusivity varies with depth near the bed-layer interface where the velocity decays exponentially to zero. Since this behavior is confined to relatively small regions at the bed-layer interface it does not appear to have a significant effect on mixing. The continuum models for flow and convective diffusion together with the correlation for the diffusivity give a robust description of transverse mixing in a rotating cylinder.

## ACKNOWLEDGMENTS

The authors are grateful for the financial support for this work from Department of Science and Technology, India, through the Swarnajayanti project.

- <sup>1</sup>P. M. Lacey, "Development in the theory of particle mixing," *J. Appl. Chem.* **4**, 257 (1954).
- <sup>2</sup>K. E. Peray, *Rotary Cement Kiln*, 2nd ed. (Chemical, New York, 1986).
- <sup>3</sup>H. Henein, J. K. Brimacombe, and A. P. Watkinson, "Experimental study of transverse bed motion in rotary kilns," *Metall. Trans. B* **14B**, 191 (1983).
- <sup>4</sup>J. M. Ottino and D. V. Khakhar, "Mixing and segregation of granular materials," *Annu. Rev. Fluid Mech.* **32**, 55 (2000).
- <sup>5</sup>R. Hogg, D. S. Cahn, T. W. Healy, and D. W. Fuersteman, "Diffusional mixing in an ideal system," *Chem. Eng. Sci.* **209**, 494 (1966).
- <sup>6</sup>S. J. Rao, S. K. Bhatia, and D. V. Khakhar, "Axial transport of granular solid in rotating cylinders. Part 2: Experiments in a non-flow system," *Powder Technol.* **67**, 153 (1991).
- <sup>7</sup>D. V. Khakhar, J. J. McCarthy, T. Shinbrot, and J. M. Ottino, "Transverse flow and mixing of granular materials in a rotating cylinder," *Phys. Fluids* **9**, 31 (1997).
- <sup>8</sup>J. M. Ottino and D. V. Khakhar, "Scaling of granular flow processes from surface flows to design rules," *AIChE J.* **48**, 2157 (2002).
- <sup>9</sup>S. B. Savage, "Disorder, diffusion and structure formation in granular flow," in *Disorder and Granular Media*, edited by A. Hansen and D. Bideau (Elsevier, Amsterdam, 1993), pp. 255–285.
- <sup>10</sup>S. B. Savage and R. Dai, "Studies of shear flows, wall slip velocities, 'layering' and self-diffusion," *Mech. Mater.* **16**, 225 (1993).
- <sup>11</sup>C. S. Campbell, "Self-diffusion in granular shear flows," *J. Fluid Mech.* **348**, 85 (1997).
- <sup>12</sup>K. M. Hill, G. Gioia, and V. V. Tota, "Structure and kinematics in dense free-surface granular flow," *Phys. Rev. Lett.* **91**, 064302 (2003).
- <sup>13</sup>S. S. Hsiau and M. L. Hunt, "Kinetic theory analysis of flow-induced particle diffusion and thermal conduction in granular material flows," *Trans. ASME, Ser. C: J. Heat Transfer* **115**, 541 (1993).
- <sup>14</sup>S. S. Hsiau and M. L. Hunt, "Shear-induced particle diffusion and longitudinal velocity fluctuations in a granular-flow mixing layer," *J. Fluid Mech.* **251**, 299 (1993).
- <sup>15</sup>S. S. Hsiau and Y. M. Shieh, "Fluctuations and self-diffusion of sheared granular material flows," *J. Rheol.* **43**, 1049 (1999).
- <sup>16</sup>S. S. Hsiau and Y. M. Shieh, "Effect of solid fraction on fluctuations and self-diffusion of sheared granular flows," *Chem. Eng. Sci.* **55**, 1969 (2000).
- <sup>17</sup>S. S. Hsiau and W. L. Yang, "Stresses and transport phenomena in sheared granular flows with different wall conditions," *Phys. Fluids* **14**, 612

- (2002).
- <sup>18</sup>J. Choi, A. Kudrolli, R. R. Rosales, and M. Z. Bazant, "Diffusion and mixing in gravity-driven dense granular flows," *Phys. Rev. Lett.* **92**, 174301 (2004).
- <sup>19</sup>C. L. Hwang and R. Hogg, "Diffusive mixing in flowing powders," *Powder Technol.* **26**, 93 (1980).
- <sup>20</sup>R. D. Wildman, J. M. Huntley, and J. P. Hansen, "Self-diffusion of grain in a two-dimensional vibrofluidized bed," *Phys. Rev. E* **60**, 7066 (1999).
- <sup>21</sup>O. Zik and J. Stavans, "Self-diffusion in granular flows," *Europhys. Lett.* **16**, 255 (1991).
- <sup>22</sup>H. Buggish and G. Löffelmann, "Theoretical and experimental investigation into local granular mixing mechanisms," *Chem. Eng. Process.* **26**, 193 (1989).
- <sup>23</sup>B. Utter and R. P. Behringer, "Self-diffusion in dense granular shear flows," *Phys. Rev. E* **69**, 031308 (2004).
- <sup>24</sup>D. Bonamy, F. Daviaud, and L. Laurent, "Experimental study of granular surface flows via a fast camera: A continuous description," *Phys. Fluids* **14**, 1666 (2002).
- <sup>25</sup>N. Jain, J. M. Ottino, and R. M. Lueptow, "An experimental study of the flowing granular layer in a rotating tumbler," *Phys. Fluids* **14**, 572 (2002).
- <sup>26</sup>A. V. Orpe and D. V. Khakhar, "Solid-fluid transition in a granular shear flow," *Phys. Rev. Lett.* **93**, 068001 (2004).
- <sup>27</sup>N. Taberlet, P. Richard, A. Valance, W. Losert, J. M. Pasini, J. T. Jenkins, and R. Delannay, "Superstable granular heap in a thin channel," *Phys. Rev. Lett.* **91**, 264301 (2003).
- <sup>28</sup>D. V. Khakhar, A. V. Orpe, and J. M. Ottino, "Surface granular flows: Two related examples," *Adv. Complex Syst.* **4**, 407 (2001).
- <sup>29</sup>J. Rajchenbach, "Dense, rapid flows of inelastic grains under gravity," *Phys. Rev. Lett.* **90**, 144302 (2003).
- <sup>30</sup>T. S. Komatsu, S. Inagaki, N. Nakagawa, and S. Nasuno, "Creep motion in a granular pile exhibiting steady surface flow," *Phys. Rev. Lett.* **86**, 1757 (2001).
- <sup>31</sup>A. V. Orpe and D. V. Khakhar, "Scaling relations for granular flow in quasi-two-dimensional rotating cylinders," *Phys. Rev. E* **64**, 031302 (2001).
- <sup>32</sup>D. V. Khakhar, A. V. Orpe, P. Andresén, and J. M. Ottino, "Surface flows of granular materials: Model and experiments in heap formation," *J. Fluid Mech.* **441**, 255 (2001).